# Ni(0) Ex-Phyllosilicates as Efficient and Stable Low Temperature CH4 Dry Reforming Catalyst

Carmen Ciotonea, Yaqian Wei, Adrian Ungureanu, Cezar Catrinescu, Olivier Gardoll, Anne-Sophie Mamede, Franck Dumeignil, Sébastien Paul, Louise Jalowiecki-Duhamel, Sébastien Royer

ChemCatChem

Research Article
doi.org/10.1002/cctc.202300245

Chemistry Europe
European Chemical Societies Publishing

www.chemcatchem.org

Special Collection

# Ni(0) *Ex*-Phyllosilicates as Efficient and Stable Low Temperature $CH_4$ Dry Reforming Catalyst

Carmen Ciotonea[+],*[a, c] Yaqian Wei[+],[a] Adrian Ungureanu,*[b] Cezar Catrinescu,[b] Olivier Gardol,[a] Anne-Sophie Mamede,[a] Franck Dumeignil,[a] Sébastien Paul,[a] Louise Jalowiecki-Duhamel,[a] and Sébastien Royer*[a]

This study explores the performances of nickel-based materials for the dry reforming of methane (DRM), an important process for hydrogen and syngas productions. Ni nanoparticles are issued from porous phyllosilicate phase exolution under reducing conditions (in situ or ex situ). Phyllosilicate precursors were obtained by deposition/precipitation with urea onto SBA-15 porous silica, with metal loading up to 40 wt.%. Reaction was performed at 600–700 °C. The successful formation and stabilization of highly dispersed nanoparticles (2–6 nm) is revealed, even for highly loaded formulations (20 wt.% and 40 wt.%). In DRM-700 ($CH_4/CO_2 = 1$, 20% $CH_4$, 480,000 mL $g_{cat}^{-1}$ $h^{-1}$) the formulation at 20 wt.% metal loading (Ni_20%) activated during reaction affords 50% and 65% of $CH_4$ and $CO_2$ conversions respectively at 700 °C. Ni_20% is showing excellent resistance toward sintering after DRM stability test of 80 h. Characterizations made for spent catalyst show high resistance toward sintering and limited carbon formation.

## Introduction

In the last decade, the global energy demand has known an important rise due to the economic development associated with the world population growth. Knowing that today the main sources of energy are still petroleum-based, the reduction of greenhouse gas (GHG) global emissions, composed to a large extent by $CO_2$, is complex.[2] Regarding in this direction, the Carbon Capture and Utilization (CCU) is aiming to convert $CO_2$ into valuable products: syngas ($H_2$ and CO), methanol, biofuels and others.[4] Hydrogen, considered as a potential energy carrier, can be produced through dry reforming of methane (DRM), this transformation presenting the interested of consuming two major GHG ($CH_4$ and $CO_2$), [Equation (1)].[1] DRM is producing syngas which is also an important feedstock for the industry.[3–9]

$$CH_4 + CO_2 \rightarrow 2CO + 2H_2 \Delta H^0_{298K} = +247\ kJ\,mol^{-1} \quad (1)$$

Nickel supported onto various supports (zeolites, $CeO_2$, $SiO_2$, $Al_2O_3$, Ce–Zr-$O_x$)[4–6] was studied for the reaction. Nickel has a relatively low cost, a high availability and presents high activity for C–C and C–H bonds cleavages.[3–22] However, when DRM is performed at high temperature, i.e. ≥ 700 °C, some problematics appear including: the instability of Ni particles, leading to significant sintering; the accumulation of carbon at the catalyst surface. Both phenomena result in productivity decrease.[3–9]

Then, the development of stable catalysts able to perform reaction at low temperature[22–24] and supporting harsh reaction conditions (high concentration of reactants, high temperature)[3–8] is particularly relevant from an industrial point of view. The preparation of high loading Ni-catalysts with high and stable dispersion, remains a great challenge. The most difficult is to achieve high dispersions over silica and alumina support surfaces over which, consequent particles reorganization and sintering occur during thermal treatment steps and reaction.[25–27] In addition, when classical impregnation methods are used, solubility of the inorganic salts and pore volume of the support are limiting the active phase loading. Consequently, it rarely exceeds 10 wt.%, except if successive impregnations are applied. At loadings above 10 wt.%, the materials are exhibiting poor dispersion, lack in homogeneity, and depressed sintering resistance, due to weak SMSI (strong metal support interaction).[23]

[a] C. Ciotonea,[+] Y. Wei,[+] O. Gardol, A.-S. Mamede, F. Dumeignil, S. Paul, L. Jalowiecki-Duhamel, S. Royer
Univ. Lille, CNRS, Centrale Lille, ENSCL, Univ. Artois, UMR 8181 - UCCS - Unité de Catalyse et Chimie du Solide, F-59000 Lille (France)
E-mail: sebastien.royer@univ-lille.fr
carmen.ciotonea@univ-littoral.fr
Homepage: https://uccs.univ-lille.fr/index.php/fr/catalyse-heterogene/matcat

[b] A. Ungureanu, C. Catrinescu
Unité de Chimie Environnementale et Interactions sur le Vivant (UCEIV, UR 4492), Université du Littoral Côte d'Opale (ULCO), 145 Av. M. Schumann, Dunkerque, 59140 (France)
Homepage: https://uceiv.univ-littoral.fr/recherche/les-equipes/catalyse/

[c] C. Ciotonea[+]
"Gheorghe Asachi" Technical University of Iasi, Faculty of Chemical Engineering and Environmental Protection, 73, Prof. D. Mangeron Bvd., 700050 Iasi (Romania)
E-mail: aungureanu@tuiasi.ro
Homepage: https://icpm.tuiasi.ro/departamente/inginerie-organica-biochimica-si-alimentara/

[+] These authors contributed equally to this work.

Supporting information for this article is available on the WWW under https://doi.org/10.1002/cctc.202300245

This publication is part of a Special Collection on "French Conference on Catalysis 2022". Please check the ChemCatChem homepage for more articles in the collection.

Promoting the formation of strong metal-support interaction (SMSI), or control over the support acid-base surface properties, are proposed to improve Ni dispersion and stability.[3–9,23,28]

The stabilization in thermo-stable phyllosilicate phase is particularly efficient. Phyllosilicates can form during impregnation processes.[29,30] However, the most adapted method remains the deposition-precipitation (DP):[28,31] 1:1 and 2:1 phyllosilicates form at slightly basic pH (pH > 7.4 ± 1) in a process involving solubilization of silicon and/or reprecipitation of silicic acid. Phyllosilicate phase formed (1:1 or 2:1) conditions material thermal stability.[31,32] Further, morphology and textural properties can be adjusted by the choice of the silica source. Use of commercial $SiO_2$ source will result in low surfaces and following activation under hydrogen is showing large particles,[33] while the use of porous materials of higher reactivity, such as MCM-41[29] or SBA-15,[30] will result in nano-phyllosilicate fibrils formation as illustrated in Scheme 1.

Use of large-pore mesoporous silica with SBA-15 topology obtained with non-ionic amphiphilic triblock copolymers as supramolecular template is particularly adapted. In this work, porous Ni(0) ex-phyllosilicate SBA-15 composites were synthesized at different metal loadings (5 wt.% to 40 wt.%) and used for the DRM reaction. At 40 wt.%, the whole silica is expected to be consumed for the crystallization of the 2:1 phyllosilicate phase. The influence of several parameters over the DRM is studied including the effect of *in situ* pretreatment to obtain active Ni(0) and reaction conditions (diluted/undiluted). Properties of synthesized Ni(0) *ex*-phyllosilicate materials are compared to reference Ni(0) over lanthanum oxycarbonate, issued from $LaNiO_3$ activation.[22,32,34,35] Material characterizations were presented over calcined, reduced and spent catalyst using $N_2$-physisorption, XPS, *in situ* XRD, TPR-$H_2$, TEM-EDXS in order to evaluate the modifications which occurred during activation and during DRM reaction.

## Results and Discussion

### Dry reforming of methane (DRM)

The reactions occurring during DRM reaction [Equation (1)] leads to a theoretical $H_2/CO$ product ratio of 1.

$$2CO \rightarrow CO_2 + C \quad \Delta H^0_{298K} = -171\ kJ\ mol^{-1} \tag{2}$$

$$CH_4 \rightarrow 2H_2 + C \quad \Delta H^0_{298K} = +76\ kJ\ mol^{-1} \tag{3}$$

$$CO_2 + H_2 \rightarrow CO + H_2O_{(RWGS)} \quad \Delta H^0_{298K} = +41\ kJ\,mol^{-1} \tag{4}$$

$$CO_2 + 2H_2 \rightarrow C + 2H_2O \quad \Delta H^0_{298K} = -90\ kJ\,mol^{-1} \tag{5}$$

$$CO + H_2 \rightarrow C + H_2O \quad \Delta H^0_{298K} = -131\ kJ\,mol^{-1} \tag{6}$$

However, depending on the catalyst and reaction conditions applied, side reactions [Equations (2–6)] can occur. The reverse water gas shift reaction [Equation (4)] leads to $H_2$ consumption. At the same time some side reactions lead to carbon production [Equations (2–3)], and even carbon plus water production through hydrogenation of carbon oxides [Equations (5–6)]. Often, the experimental $H_2/CO$ ratio differs from 1. If water is produced, as a result of side reactions, WGS reaction can also eventually participate.

### Effect of pretreatment temperature in $H_2$

In a first step, metallic catalysts are produced as classically performed, meaning applying a first step of activation under pure $H_2$ flow at T = 600–700 °C for 10 h. Then, Ni_20% and Ni_40% where activated under the defined conditions. DRM reaction in diluted conditions at 600 °C (DRM-600 °C) and 700 °C (DRM-700 °C) are presented in Figure 1 and Figure S2. The pretreatment temperature noted as zero corresponds to a catalyst used calcined, without any activation step prior to the DRM test. The results are showing that without *in situ* pretreatment, Ni_20% catalyst, allows reaching conversion $X_{CH4} = 25\%$ and of $X_{CO2} = 35\%$ for DRM at 600 °C. For higher temperature, DRM at 700 °C, higher conversion was obtained, $X_{CH4} = 50\%$ and $X_{CH4} = 65\%$, while scarce carbon formation is identified (Table S1). For the Ni_20% catalyst, slightly better conversions (for both $CH_4$ and $CO_2$) are obtained applying a $H_2$ pretreatment at 600 °C or 650 °C before DRM reaction. However, when using Ni_40%, such pretreatment leads to an opposite trend, with a small decrease of both conversions, an effect more marked for DRM-600 °C. This may be explained by the fact that the fast reduction is inducing

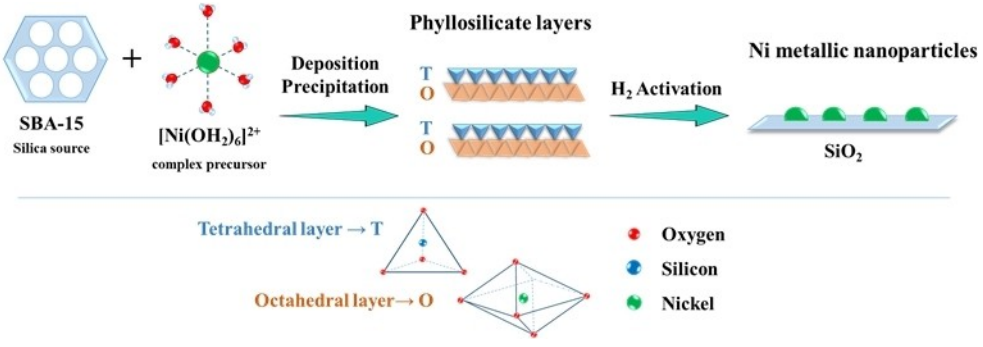


**Scheme 1.** Schematic view of the synthesis approaches for the preparation of Ni-ex phyllosilicate catalysts. (Adapted from ref. [31])

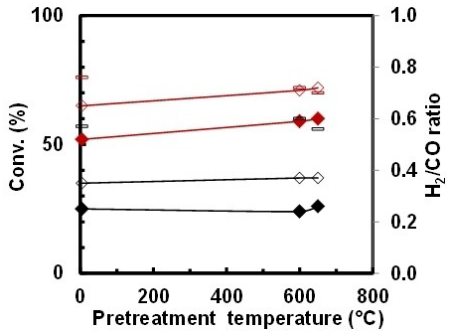


**Figure 1.** Conversions of $CH_4$ (◆) and $CO_2$ (◇) and $H_2$/CO ratio (▭) as a function of pretreatment temperature in $H_2$. Results obtained at T = 600 °C (black), T = 700 °C (red). (a) Ni_20%. Conditions: 10 mg of catalyst, $CH_4$/$CO_2$ = 1, $CH_4$ and $CO_2$ at 20%, 480,000 mL $gcat^{-1}$ $h^{-1}$. Values measured after 5 h in reaction.

the appearance of fewer active centers, mainly when the Ni is embedded within many filaments of the phyllosilicate, thus the accessibility to the reduction is limited, especially for high metal loading. As expected, the $H_2$/CO ratio is dependent on reaction temperature. This ratio is slightly affected by any pretreatment. For DRM-600 °C, whatever the pretreatment temperature and the catalyst used, the ratio is of ~0.57–0.63. Instead, for DRM-700 °C, the $H_2$/CO ratio is slightly increasing to 0.72–0.78. Knowing that these tests were performed under relatively diluted conditions (namely $CH_4$ at 20 vol.% of the feed), the carbon balance is always measured above 90% whatever the reaction temperature and the catalyst used. Moreover, we noticed no carbon accumulation (Table S2), unless for Ni_40% when the reaction is performed without pretreatment. The carbon production rate of carbon over Ni_40% is in relatively good agreement with the higher value of 0.0097 g $g_{cat}^{-1}$ $h^{-1}$obtained by TGA analysis (Table S2). As a matter of fact, even though the TGA analysis involves only a small quantity of compound, is allowing to determine a total quantity of carbon formed after the reforming reaction. Therefore, the treatment under $H_2$ allows decreasing carbon formation, and is beneficial in such a way for the DRM reaction. It is important to remark that under these conditions in most cases, similar conversions are obtained with and without pretreatment, while avoiding a pretreatment allows economizing energy. As conclusion, a treatment temperature of 600 °C under $H_2$ seems appropriate, as it allows decreasing carbon formation for high Ni loading catalyst, even if it decreases slightly the conversion, although for lower Ni content catalysts it allows increasing slightly the conversion. This is in agreement with the literature where pretreatment steps are generally conducted at temperatures sufficiently high to ensure complete reduction of $Ni^{2+}$ species (~700 °C).[3–9,25,36] Previously, on Ce–Ni based catalysts, it was observed that an "in reaction" reduction of the catalyst resulted in higher rates of carbon accumulation.[37]

However, the influence of catalyst reduction in different environments was analyzed, and different behaviors were observed depending on catalysts nature.[9]

### Effect of nickel content

The influence of Ni content in Ni_X% catalysts was evaluated over DRM-t reaction. The catalytic test was conducted with or without pretreatment at 600 °C. The results obtained on the Ni_5% and Ni_40%, without pretreatment are presented in Figure S1, the results are plotted versus Ni–X%, in Figures 2 and (in situ treatment at 600 °C) and S3 (without treatment). Regarding the time on stream, a higher decrease of the conversions is obtained on the low Ni content compound for DRM-700, while in the other cases only slight decrease is obtained, with stable conversions after 5 h (Figure S3). When the Ni content increases up to 20 wt.%, both $CH_4$ conversion and $CO_2$ conversion are observed to increase whatever the conditions of pretreatment, (Figures 2 and S3). Thereafter, only small conversion changes are observed between

Ni_20% and Ni_40%. As an example, reaction conducted without pretreatment over Ni_40% leads to the highest conversions: $X_{CH4}$ = 27%, $X_{CO2}$ = 37% for DRM-600 °C; $X_{CO2}$ = 68% for DRM-700 (Figure S1). The $H_2$/CO ratio remains lower than 1 whatever the Ni loading and temperature range, even if it is slightly affected by the temperature: $H_2$/CO ratio = 0.7 at 600 °C, and close to 0.8 at 700 °C (Figure 2). Globally, the conversions are not varying very much with the Ni loading. Two parameters can be at the origin of this result: (1) reduced accessibility to active sites located on exposed nanoparticles over highly loaded catalysts; (2) progressive decrease of metal dispersion when metal loading increase.[38] Albarazi et al.,[36] who studied the DRM reaction over X wt.% (X = 5 to 15) Ni on $CeO_2$-$ZrO_2$/SBA-15 catalysts, observed comparable phenomenon: at 600 °C, the 10 wt.% and 15 wt.% Ni samples present comparable $CH_4$ conversions at ~60% ($CH_4$:$CO_2$:Ar = 1:1:8, 20,000 mL $h^{-1}$ $g_{cat}^{-1}$). The $Ce_{0.75}Zr_{0.25}O_2$ mixed oxide modified samples however present better stabilities compared to the unmodified Ni/SBA-15 compounds, which showed evident deactivation. The $H_2$/CO ratio obtained here is similar at high temperature but lower at 600 °C.

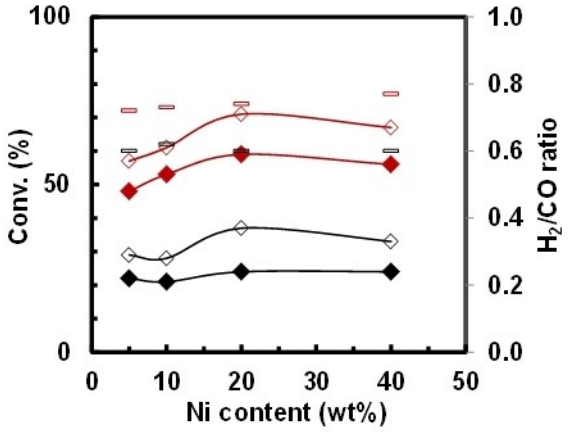


**Figure 2.** Conversions of $CH_4$ (◆) and $CO_2$ (◇) and $H_2$/CO ratio (▭) as a function of Ni content. The catalysts are *in situ* pretreated under $H_2$ flow at 600 °C before reaction. Results obtained at T = 600 °C (black) and T = 700 °C (red). Conditions: 10 mg of catalyst, $CH_4$/$CO_2$ = 1, $CH_4$ and $CO_2$ at 20%, 480,000 mL $g_{cat}^{-1}$ $h^{-1}$. Values measured after 5 h in reaction.

On 12 wt.% Ni/Ce-SBA-15 (Ce/Si = 0.04) compound, Wang et al. reported in DRM at 700 °C ($CH_4/CO_2 = 1$, and 36,000-mL $h^{-1}$ $g_{cat}^{-1}$), $X_{CO2} = 75.7\%$ and $X_{CH4} = 75.2\%$, conversions which remained almost constant during 40 h of reaction even if the formation of filamentous carbon was evidenced.[28]

### Performance for Ni_20% under diluted conditions ($CH_4$ at 20%)

Considering the results from Section 3.1.2 we select for the next tests to continue with the diluted condition and to use a higher mass of Ni_20% catalyst of 50 mg, without pretreatment in DRM-t, (96,000 mL $g_{cat}^{-1}$ $h^{-1}$), not only to analyze the catalytic performance but also to get enough compound to allow performing after test physico-chemical characterizations. The $CO_2$ and $CH_4$ conversions decrease with time and become relatively stable after few hours (Figure 3). Indeed, $X_{CH4} = 46\%$ and $X_{CO2} = 50\%$ are initially measured, and they gradually decline with time, by approx. 8%, during the 5 h of DRM-600. After 5 h of DRM-600 °C, $X_{CH4} = 36.7\%$ and $X_{CO2} = 44.3\%$, while the $H_2$/CO ratio stabilizes at 0.74. For DRM-700, after 5 h of reaction the $CH_4$ and $CO_2$ conversions are of $X_{CH4} = 68.7\%$ and $X_{CO2} = 77.8\%$, respectively. Only slight decrease (4%) compared to the initial conversions is observed and a stable $H_2$/CO ratio of 0.78 is obtained. At the end of the reaction cycle (600 °C followed by 700 °C), ~ with a rate of carbon accumulation of 0.110 g $g_{cat}^{-1}$ $h^{-1}$. Therefore, in comparison to the results reported here before, as expected, a higher carbon formation rate is obtained when the mass of catalyst is increased (50 mg compared to 10 mg) for DRM-700 °C, which is related to the higher conversions obtained.

The results reported here can be compared with those reported recently by Li and al.[22] $5Ni/La_2O_2CO_3$-$Al_2O_3$ compound which allowed obtaining 62% of $CH_4$ conversion at 650 °C ($CH_4/CO_2/N_2 = 15/15/70$, 240,000 mL $h^{-1}$ $g_{cat}^{-1}$, $CH_4$ GHSV of 3.6 $10^4$ $h^{-1}$) evidenced high performance in a comparison Table of Ni based catalysts (including perovskite catalyst) when taking into account $CH_4$ GHSV. For easy comparison, in the present study, $CH_4$ GHSV of 9.6 $10^4$ $h^{-1}$ corresponds to conditions: $CH_4$ and $CO_2$ at 20% and 480,000 mL $g_{cat}^{-1}$ $h^{-1}$. For low reaction temperature of 600 °C, a $CH_4$ conversion of 65% was previously reported on $10Ni/La_2O_3$ (with $CH_4$ GHSV of 1.2 $10^4$ $h^{-1}$).[22,24] Qian et al.[39] synthesized SBA-15 supported Ni catalyst (6 wt.%), and evaluated the catalyst properties for DRM reaction (conditions: T = 600 °C, catalyst weight = 45 mg; $F_{tot} = 15$ mL $min^{-1}$, $CH_4/CO_2 = 1$, $[CH_4] = 20$ vol.%). $CH_4$ conversion of 28% and $CO_2$ conversion of 34% were obtained after 1 h of reaction at 600 °C. At 700 °C, the catalyst allowed getting 53% of conversion of $CH_4$ and 58% of conversion of $CO_2$. $H_2$/CO ratio was increasing with reaction temperature, still remaining below 1: 0.73 (T = 600 °C), 0.81 (T = 700 °C). Omoregbe et al.[40] reported on 10 wt.% Ni/SBA-15 compound (24,000 mL gcat$^{-1}$ $h^{-1}$, 150 mg of catalyst) 48% and 60% for $CH_4$ and $CO_2$ conversions, respectively in DRM reaction at 650 °C. Consequently, the Ni_X% catalysts presented in this work are showing high performances considering that more severe conditions are applied (low mass of catalyst and/or high flow rate), while limited carbon formation occurs compared to literature [9] in particular when considering the high Ni loading catalyst and the absence of doping element in the formulation.[28,36] Indeed, Ni/SBA-15 deactivated during DRM when reaction temperature increased ($CH_4/CO_2/Ar = 1/1/8$, 20,000 mL.$h^{-1}$ gcat$^{-1}$): $XCH_4 = 57.5\%$ at 600 °C, reducing to 52% at 630 °C.[36] Ceria-zirconia modified samples showed better stability, even if a carbon nanofibers accumulation on the catalyst was observed.[37] Even if Arcotumapathy et al.[41] observed a limited carbon accumulation in Ni/SBA-15 catalyst during methane steam reforming (SRM), leading to good resistance toward carbon deposition compared with $Ni/Al_2O_3$, DRM reaction is also known to promote a higher carbon formation compared to SRM.[3–9]

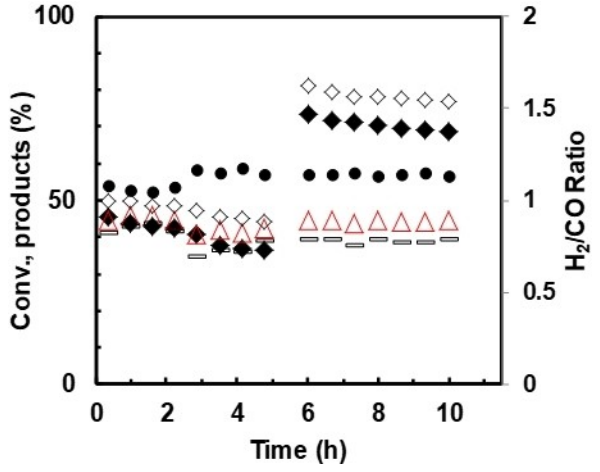


**Figure 3.** Conversions of $CH_4$ (◆) and $CO_2$ (◇), products formation ($H_2$ (△) and CO (●)) and $H_2$/CO ratio (▭) obtained with Ni_20% catalyst without pretreatment. Reaction performed at T = 600 °C and T = 700 °C. Conditions: 50 mg of catalyst; $CH_4/CO_2 = 1$, $CH_4$ and $CO_2$ at 20%, 96,000 mL gcat$^{-1}$ $h^{-1}$.

### Performance of Ni_20% under undiluted conditions (harsh conditions)

The performance of the Ni_20% compound (10 mg) *in situ* pretreated under $H_2$ at 600 °C was measured for DRM-600 under undiluted feed gas composition (50% $CH_4$–50% $CO_2$, with 480,000 mL $g_{cat}^{-1}$ $h^{-1}$). The obtained results are reported in Figure 4 and Table S1. For deep analysis, the mass of catalyst and gas flow are adapted to avoid reaching thermodynamic limit for better comparison with the classical $LaNiO_3$ catalyst. Figure 4 shows that the catalyst activity is stable at least for 5 h: $X_{CH4} = 21\%$, $X_{CO2} = 26\%$ and $H_2$/CO ratio = 0.7, with accumulation rate of carbon measured at 0.08 g $g_{cat}^{-1}$ $h^{-1}$. Then, in severe conditions, carbon is formed on Ni_20% and Ni_40% compounds. For comparison, the results obtained in the same conditions on $LaNiO_3$ (Figure S4) are evidencing lower conversions of both reactants and decreased $H_2$/CO ratio. The high performance in DRM of nickel - SBA-15 mesoporous silica composite has already been highlighted previously, by comparison to the classical LaNiO3 catalyst.[32] $LaNiO_3$ perovskite catalyst has been reported for a long time as active for DRM reaction,[42] and several

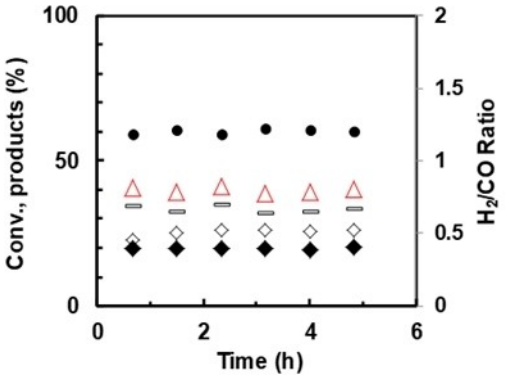


**Figure 4.** Conversion of $CH_4$ (◆) and $CO_2$ (◇), products formation ($H_2$ (△), CO (●)), and $H_2$/CO ratio (▭) obtained with Ni_20% catalyst pretreated under $H_2$ at 600 °C. Reaction performed at T = 600 °C. Conditions: 10 mg of catalyst, $CH_4/CO_2 = 1$ and 50% $CH_4$, 480,000 mL $gcat^{-1}$ $h^{-1}$.

researchers tried to find an active and stable perovskite formula[3–24,43] which remains an open challenge considering the progressive sintering of the metallic Ni NPs on the surface of the lanthanum oxycarbonate phase in the course of the reaction. On a novel sandwiched core–shell structured Ni-$SiO_2$@$CeO_2$ catalyst, where Ni-phyllosilicate was used as the Ni precursor producing highly dispersed Ni nanoparticles on $SiO_2$, Das et al. attributed primarily the higher activity of the catalyst to the higher Ni dispersion.[11] In their study the Ni-$SiO_2$ catalyst (~9 Ni wt %) without the $CeO_2$ coating, used for comparison, showed low activity at 600 °C in undiluted model biogas $CH_4/CO_2$ of 3:2 (200 L $h^{-1}$ $g_{cat}^{-1}$) and extensive coke formation.

### Stability test for Ni_20%

Ni_20% was used to perform the stability test for a total duration of 80 h of DRM reaction for Ni_20%. The results are presented in Figure S9 and are showing that Ni_20% is expose an excellent stability for such long time for performing the DRM reaction. After the 80 h, there are measured the conversions for $CO_2$ of 79% and $CH_4$ of 50%, while the ratio $H_2$/CO is maintained stable at 0.77. The sample collected after the catalytic test was analyzed by XRD and ATG and the results are presented in Figures S10 and S11. As it can be observed, after 80 h of stream on the diffractogram is present an intense peak at 2θ of 26°, which is associated to the presence of carbon graphite. Concerning the Ni, the average crystallite size couldn't be measure as both $Ni^0$ and carbone are showing the peak at 2θ at 44,5° and 44,55°, nevertheless is can be observed that the peaks at 2θ of 51.8° and 76.3° are broad and of very low intensity suggesting the presence of dispersed and small crystallites. Concerning the formation of carbon, the presence of carbon graphite is revealed also by presence of the peak at 648 °C, typical for the decomposition o graphitic like carbon, during the thermogravimetric analysis (Figure S13), the weight loss registered after 80 h of reaction under the conditions mentioned in the legend of Figure S9 is of 42 wt.%. Comparing our results with the work of Korasi et al,[43] which obtained up to 30% of carbon for the stability test of 50 h at 750 °C for Nickel-$SiO_2$ catalyst we can consider that Ni_20% is showing high resistance toward the carbon formation.

### Characterization study

#### *Catalysts in the oxidized state*

Characterizations of solids were performed before and after reduction in order to evaluate the interest of using Ni inserted into phyllosilicate phase to improve the dispersion of the metallic Ni particles in the catalyst after activation. The wide-angle XRD patterns obtained for Ni_X% catalysts are presented in Figure S4. All the patterns show broad peaks at 2θ of 35°, 60° and 70°. These reflections are associated to the kerolite phase like 1:1 type phyllosilicate (ICDD reference 43–0664). Kerolite is of chemical formula $Ni_3Si_4O_{10}(OH)_2\,5H_2O$.[29,31,45] Considering that the nickel loading is progressively increased up to 40 wt.%, the talc structure of 2:1 phyllosilicate type is expected to be formed at high loading, in addition to the 1:1 phyllosilicate type. Indeed, when classically synthesized, *i.e.* using hydrothermal approach, pure 2:1 phyllosilicate phase is obtained, it was easily confirmed by XRD (Figure S4). The X-ray diffraction alone is not showing conclusive information about the presence of T:O:T layers. In addition, as illustrated in the micrographs presented in Figure S5,[46] the presence of broad reflections at 2θ ~ 70–75° may be an indication of this possible formation of 2:1 phase only for Ni_20% and Ni_40%. Finally, when compared with the PS 2:1 sample, synthesized using hydrothermal approach, the diffractogram of Ni_40% is characterized by less intense and broader reflections. As an example, while the (0 6 0) reflection (located at 60.87°) of the PS 2:1 sample presents a FWHM of 1.280, the (3 3 0) reflection (located at 60.77°) of Ni_20% and Ni_40% presented FWHM of 1.483 and 2.622, respectively. These observations are indications of smaller crystal domain size for the phyllosilicates formed by DP over SBA-15 than using conventional hydrothermal synthesis.[33] Finally, $LaNiO_3$ perovskite, prepared as catalyst reference, presents pure $LaNiO_3$ phase of trigonal structure according to the ICDD reference 033–0711.We select for this work, the reference of $LaNiO_3$, as is a material often used for DRM reaction and is reported in many studies from the literature.[43] TEM analyses were performed on Ni_X% calcined samples to inform on morphological material characteristics (Figure S6). The images allows the identification of fibrillar-like particles, characteristic of phyllosilicate phases.[47] EDXS analysis, performed on silica grain scale allowed to point the incorporation of Ni element in the fibrillary particles, without formation of any bulky individual NiO NPs that are usually observed when wet or incipient wetness impregnations are used for the supported catalysts preparations.[30,47,48] When the Ni loading increases, the following evolutions can be observed: (i) the porosity ordering of the SBA-15 support is becoming less defined, and when the 40 wt.% of nickel is reached, residual hexagonal pore ordering on large scale is absent on the observed zones; (ii) the quantity of observable fibrillar-like

particles is increasing, as well as the length of the filaments (size mostly $<50$ nm for Ni_5% to mostly $>200$ nm for Ni_40%); (iii) larger filaments seem to grow on the periphery of the silica grains, given to an urchin-like morphology while small filaments are also observed in the internal porosity of the silica grains.

This morphological evolution is reflected on the textural properties as measured by $N_2$-physisorption at $-77$ K (Figure S7 for the isotherms and pore diameter distribution, textural properties listed in Table 1). The isotherm obtained for the SBA-15 support (Figure S7) is of type IV: a saturation plateau is observed at high $P/P_0$ which corresponds to the capillary condensation phenomenon occurring in mesopores. H1-type hysteresis, with parallel and vertical adsorption and desorption branches, is also observed. This reflects the formation of mesopores in the solids having cylindrical pores of regular shape and size. Type IV isotherms are always obtained over the Ni_X% materials, until 20 wt.% Ni, with a progressive shortening of the capillary condensation plateau length with the increase of the metal loading. The progressive shortening of the plateau associated to the shifting of the adsorption and desorption steps toward the higher $P/P_0$ characterizes the formation of a second porosity of larger size in the Ni_X% samples, compared to the SBA-15 support. In addition, the change in the hysteresis shape to a $H_3$ type evidences a loss in pore homogeneity. In the case of the Ni_40%, a significant delay in $P/P_0$ desorption occurs, and it characterizes the formation of slit-shaped pores as classically observed in lamellar materials.[45] Then, and as expected from XRD and TEM results, a progressive transformation of the SBA-15 pore network occurs with the metal loading increase, at the expense of the fibrillar-type phyllosilicate phase formation. The PS phase formation involves, as described by several authors,[27,31] silica dissolution in basic conditions, with reprecipitation step of metal and silicon cationic species into lamellar brucitic phase of the phyllosilicate. Such mechanism obviously leads to the consumption of the SBA-15 during dissolution-precipitation process. The progressive transformation of the SBA-15 support into phyllosilicate phase has a significant effect on the textural properties (Table 1). First, on the specific surface areas, a significant decrease is observed with the insertion of nickel. While a surface area exceeding 700 $m^2 g^{-1}$ is observed for the SBA-15 initial phase (as typically reported,[30]), surface areas from 306 to 363 $m^2 g^{-1}$ are obtained over the Ni_X% without any clear trends of evolution with the metal loading (all Ni_X% samples show $-51$ to $-58$% surface area decrease). Nevertheless, values similar for Ni_X%, may be explained by the random consumption on the outside and either inside the grain of SBA-15. Also, we observe that the percentage of nanofilaments together with the presence of larger pores is progressively increasing when the metal loading is increasing, thus the total specific surface is resulting in similar values for Ni_5% to Ni_40%. The micropores volume, initially found on the parent SBA-15 is also significantly reduced, dropping from 119 $m^2 g^{-1}$ for SBA-15 to 61–66 $m^2 g^{-1}$ for all Ni_X%. Analyzing the pores volume allows evidencing that 13% to 20% pores volume decreases are obtained for samples with Ni loading below or equal to 20% for which the isotherms present hysteresis of comparable shape to the one obtained on the SBA-15 initial material. In the case of Ni_40%, for which hysteresis suggests the formation of slit-shaped pores, a more pronounced decrease in pores volume is noted. However, Ni_40% maintains 1.6 times higher surface area compared to PS 2:1 sample, as well as a pores volume 2 times higher.

The results of XPS analyses performed on the Ni_5% and Ni_20% calcined materials are presented in Figure 5 and Table S2. Ni $2p_{3/2}$ component located at 856.6 eV (Table S2), with its satellite located at 862.6 eV[49] is showing the presence of $Ni^{2+}$ species. Indeed, the BE reported previously by Lehmann et al. for 1:1 phyllosilicate[29] was of 856.6 eV. The O 1s core level (presented for Ni_5% and Ni_20% in Figure 5) presents two major contributions of 532.9 eV. The contribution at 532.9 eV is associated to $O^{2-}$ species from silica framework. For pure phyllosilicate phases is often labeled the contribution at 531.5 eV, ascribed to oxygen species form –OH groups from the phyllosilicate layers. The spectra recorded the Ni_X% are showing very small shoulder that may be associated to 531 eV, this may be due to the presence of fewer filaments that contain the –OH groups at the surface of the materials analyzed. The Si 2p peak at 103.3-103.6 eV is associated to the presence of Si–O bonds.[50] The difference in binding energies Ni $2p_{3/2}$-Si 2p was used to determine the interaction between Ni and Si species.[51, 52] In ref.,[53] it was proved that a BE difference from 753.2 eV and

**Table 1.** Textural properties and reduction characteristics of Ni_X% samples (samples calcined at 500 °C).

| Sample | $N_2$ physisorption | | | | $H_2$ temperature programmed reduction | | | % atoms at NP surface[d] |
|---|---|---|---|---|---|---|---|---|
| | $S_{BET}$/[a] $m^2 g^{-1}$ | $S_\mu$/[a] $m^2 g^{-1}$ | $V_p$/[a] $cm^3 g^{-1}$ | $D_p$/nm | Temp. of red/ °C | H2 consump./ mmol $g^{-1}$ | Ni red degree/[b] % | |
| SBA-15 | 735 | 119 | 1.02 | 6.7 | – | – | – | – |
| Ni_5% | 353 (−52%) | 65 | 0.82 (−20%) | 7.5, 8.3 | 620 | 0.81 | 95 | 33.1 |
| Ni_10% | 306 (−58%) | 64 | 0.89 (−13%) | 8.0, 13.0 | 620 | 2.21 | 89 | 31.5 |
| Ni_20% | 346 (−53%) | 66 | 0.86 (−16%) | 8.3, 11.5 | 622 | 3.13 | 92 | 29.7 |
| Ni_40% | 363 (−51%) | 61 | 0.60 (−41%) | 4.1 | 640 | 6.06 | 89 | 32.3 |
| PS 2:1 | 220 | 0 | 0.27 | 3.7, 4.3 | 780 | 6.12 | 98 | 13.6 |
| $LaNiO_3$ | 7.9 | – | – | – | 300, 339, 497 | 5.14 | 85[c] | – |

[a] Parenthesis: percentage of decrease compared to the SBA-15 initial support. [b] Calculated on the reaction $Ni^{2+}$ to $Ni^0$. [c] Calculated on the reaction $Ni^{3+}$ to $Ni^0$. [d] % of atoms exposed on the surface, calculated using the particle sizes determined by TEM statistical analysis, considering that dNi = 0.84 × dNiO based on the differences of molar mass and density, and that for each particle, Ni dispersion (%) = 97.1/dNi (nm).[34] [d] anchored in top row, right column. Then, the approach applied allows obtaining far better textural properties than those obtained over classical PS 2:1 sample prepared by hydrothermal synthesis.

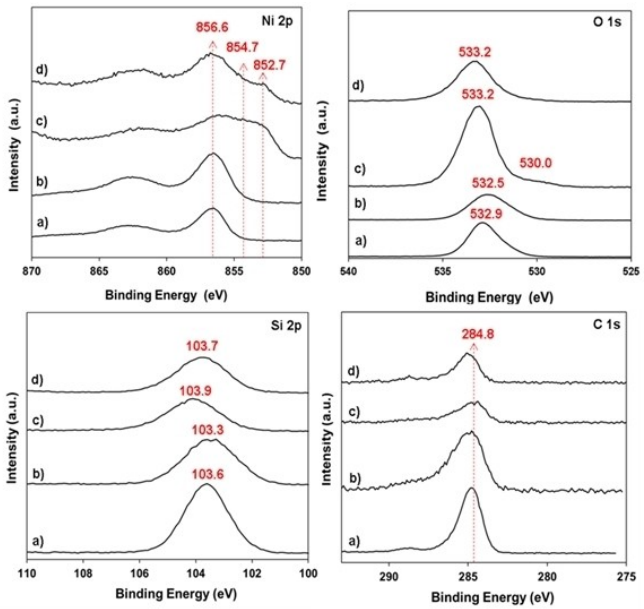


**Figure 5.** XPS Ni $2p_{3/2}$, C 1s, O 1s, and Si 2p spectra obtained for Ni_5% (a) and Ni_20% (b) samples calcined at 500 °C, Ni_20% sample after treatment under $H_2$ at 700 °C (Ni_20_red700, c), and Ni_20% after DRM reaction performed at 700 °C ($CH_4/CO_2 = 1$, 20% of $CH_4$, without *in situ* pretreatment in $H_2$) (Ni_20%_after test, d).

753.6 eV is characteristic of nickel silicates presence. The values identified here on the two selected materials are of 753.0 eV and 753.3 eV, which supports the formation of nickel silicates. Finally, the C 1s signals are composed of 3 contributions, the major one being associated to adventitious carbon at 284.8 eV. Residual hydroxyl and carbonylic/carboxylic species can be identified by low intensity signals at BE of 286.3 eV and 288.6 eV, respectively. Such residual species can also originate from external contamination.

### *Catalysts under reducing conditions*

Nickel ion reducibility in Ni_X%, PS 2:1 and $LaNiO_3$ was evaluated using $H_2$-TPR (Figure 6), and characteristic values obtained from the experiments are listed in Table 1. Reduction occurs in one main step, being located at 780 °C for the PS 2:1 reference sample, and at lower temperature (620–640 °C) for the Ni_X% samples. Temperature of reduction observed for PS 2:1 sample is typical of the reduction of 2:1 phyllosilicate, for materials having a large number of alternating T:O:T layers.[45] At the opposite, the reduction at lower temperature observed for the Ni_X%, by ~150 °C, demonstrates the higher reducibility of the phases formed in Ni_X%. Two phenomena can be at the origin of this decrease of temperature: (i) the decreases of the filament stacking and in filament sizes; (ii) the formation of 1:1 phyllosilicate,[45] as previously concluded from XRD analysis.

Quantification of the hydrogen consumed on the whole temperature range shows consumptions varying from 0.81 to 6.06 mmol $g^{-1}$ (depending on Ni loading in the sample), leading to Ni reduction degrees of 89–95% for all materials that confirms analmost complete reduction of Ni contained in the materials. Comparable result is obtained for the PS 2:1 sample, for which a reduction degree of 98% is obtained from $H_2$ consumed quantity). Evolution of the materials structure with temperature and under $H_2$ flow was followed by in situ XRD (Figure 7). For the Ni_X% samples, the reflections assigned to the kerolite type 1:1 phyllosilicate phase (located at 2θ of 35° and 60°) are visible up to 600 °C. The TPR experiments showed that at 600 °C, some Ni cations were already reduced. When the temperature of reduction reaches 800 °C, the reflections of the phyllosilicate phase completely disappear or they are significantly attenuated. According to the TPR experiments, at 800 °C, reduction of Ni cations to metal ($Ni^0$) is achieved that explains why the signal for phyllosilicate can no longer be observed. For Ni_5% and Ni_10% samples, the absence of clear signal for metallic phase formation, up to reduction temperature of 800 °C, suggests the presence of well dispersed metallic nickel phase. The obtaining of metallic nickel ($Ni^0$) particles is revealed for higher loading samples (i.e.

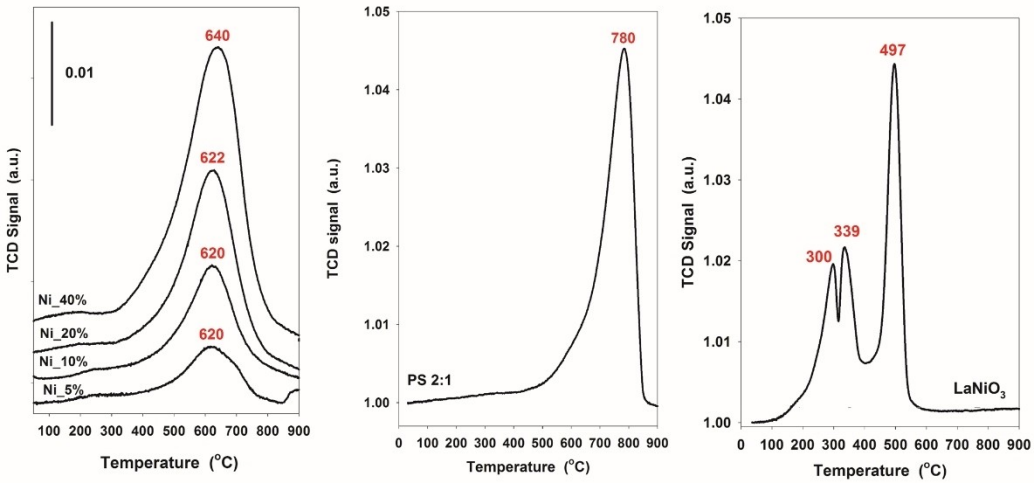


**Figure 6.** $H_2$-temperature programmed reduction obtained for Ni_X% catalysts (left); 2:1 Ni-phyllosilicate reference (middle); $LaNiO_3$ reference catalyst (right).

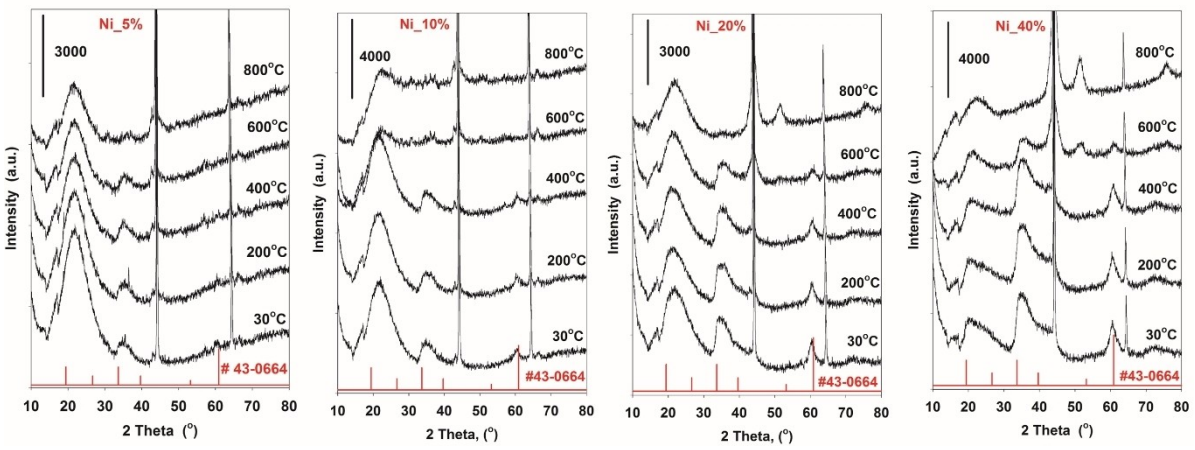


**Figure 7.** In situ XRD experiments for calcined Ni_X% samples (reducing treatment performed under 5% $H_2$ in Ar flow).

Ni_20% and Ni_40%) with broad diffraction signals located at 52.04° and ascribed to cubic $Ni^0$ phase (ICDD 04–0850). Applying the Scherrer equation to the observable reflections leads to average crystallites sizes below 6 nm: 4.4 nm (Ni_20%), 5.2 nm (Ni_40%).

Ni_X% samples were analyzed by TEM after a treatment under $H_2$ at 600 °C and 800 °C. Ni nanoparticles originate from phyllosilicate phases are resulting by sintering from the octahedral layer of the phyllosilicate where the Ni atoms were positioned, as illustrated in Scheme 1. By the location of the filaments, is found that the NPs are disposed either outside the silica, occupying the place where the filaments were and as well inside the porosity where some nanolayers of phyllosilicates were formed within the open porosity of the SBA-15. For 600 °C, temperature at which hydrogen starts to be consumed (by TPR), and at which *in situ* XRD demonstrates the partial maintaining of phyllosilicate fibrous structure, TEM analysis (Figure 8) evidences: i) the presence of metallic Ni NPs and ii) remaining phyllosilicate filaments. Comparable observation is done whatever the metal loading in the sample, except that metallic NPs formed is becoming easier to be observed with the increase in nickel loading. NPs produced are mostly located at the periphery of the silica grains in low loading samples, and their repartition equilibrates throughout the silica grains in high loading samples. After treatment in $H_2$ at 800 °C, almost all $Ni^{2+}$ contained in the samples is supposed to be reduced to metal (position after TPR peak in Figure 6; absence of phyllosilicate reflections in Figure 7). TEM showed a limited sintering of the metallic NPs (Figure 8), with histograms showing populations of particles centered at 3–5 nm and no visible particles of size exceeding 10 nm. These values are in agreement with the values observed from X-ray line broadening. Considering the temperature of treatment applied, of 800 °C, it demonstrates an excellent resistance of the materials to the sintering phenomenon. Indeed, when a poor interaction between the silica support surface and the nickel phase exists, NPs are growing significantly, up to 10 nm (when confined in mesopores) and largely above if no confining occurs.[53] For the classical hydrothermal synthesized PS 2:1 reference, a significantly larger Ni NPs size is obtained after reduction at 800 °C, with a wide repartition in size (Figure 8, mostly from 5 nm to 17 nm) confirming a lower resistance to sintering of this material, when compared to Ni_X% materials.

TPR profile of $LaNiO_3$ (Figure 6) shows two main reductions steps:

- the low temperature consumption, composed of two successive contributions, is assigned first to the reduction of $Ni^{3+}$ into $Ni^{2+}$ (the first contribution with a maximum at 300 °C, is due to the possible formation of $La_2Ni_2O_5$) followed by the reduction of a part of formed $Ni^{2+}$ into $Ni^0$ (second contribution with a maximum at 339 °C, $Ni^{2+}$ located on the surface and in the grain boundaries).
- the high temperature consumption, located at 497 °C, and assigned to the reduction of residual $Ni^{2+}$ into $Ni^0$. These results are in line with previous reports,[26] and the amount of hydrogen consumed allows calculating a reduction of $Ni^{3+}$ to $Ni^0$ of 85%, which demonstrates when a temperature of 900 °C is applied an almost complete reduction of whole Ni cations from the perovskite, assuming a small proportion of $Ni^{2+}$ are stabilized in the calcined initial structure.

The XPS analyses performed on the Ni_20% sample treated in $H_2$ at 700 °C (noted Ni_20%_r700, Figure 5, Figure S14 and Table S3) show the presence of Ni species at different oxidation states and in different environments. In Table S2, Ni $2p_{3/2}$ peak is decomposed using contributions at 856.6 eV and 854.7 eV, in agreement with the formation of $Ni^{2+}$ species, with the same binding energy as previously observed on the calcined compounds and one like in NiO phase.[29,49] Metallic nickel ($Ni^0$) is clearly evidenced with a contribution at 852.9 eV appearing after treatment in $H_2$ at 700 °C, even if the material has been exposed to air before XPS analysis.[49] As reported in Table S2 the $Ni^0$/ $Ni^{2+}$ surface ratio is found to be lower than 0.3 (the uncertainty on the value is due to poor spectral resolution). The O 1s core level spectra is composed of one major contribution at 533 eV (Figure 5) which can be associated to the oxygen species in $SiO_2$, and of a small contribution at 530 eV associated to $O^{2-}$ from NiO phase.[50] The Si 2p peak at 103.9 eV confirms

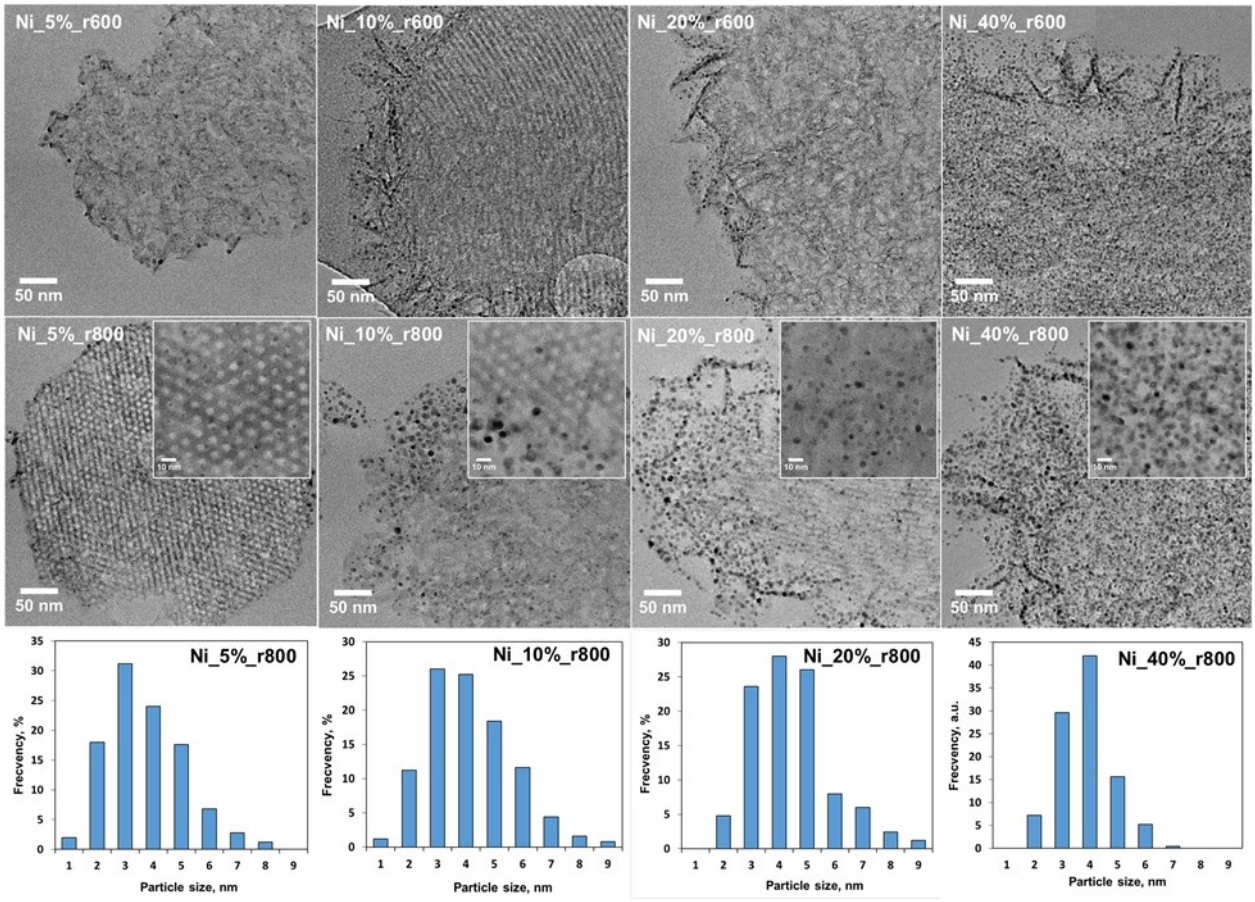


**Figure 8.** TEM images collected for the Ni_X% samples reduced at 600 °C and 800 °C; histograms of particles size obtained after reduction at 800 °C.

the presence of Si–O bonds while the difference in binding energies of Ni and Si ($Ni2p_{3/2}$ -Si2p) is measured at 752.4 eV confirming a partial maintaining of nickel silicate phases.

### Catalyst evolution under reaction

In this section there will be depicted the results for the catalytic performances in relation with the results obtained for the spent catalyst. As previously observed in Figure S1, the Ni_X% catalysts display good stabilities in reaction (after 5 h) even if some deactivation still occurs on the Ni_5% catalyst. The catalysts have been characterized by TEM after tests (Figure 9) and the following observations can be done:

(i) The catalyst morphology, on a micrometric scale is not affected by the reaction (5 h at 600 °C followed by 5 h at 700 °C). Indeed, the Ni_5% always shows hexagonal pores ordering at long range. For the higher loading samples (Ni_20%, Ni_40%), the urchin-like morphology is always observed, with larger fibrillary PS phase always located on the periphery of the silica grains.

(ii) The Ni NPs do not suffer from significant sintering. Indeed, comparison between histograms before reaction (Figure 8) and after reaction (Figure 9) shows that the Ni average particles size shifts by less than 0.5 nm for Ni_5% and majority in the range of 3 and 5 nm with fewer particle larger of 7 nm. In the case of Ni_20% and Ni_40%, the Ni average particles sizes increase after the catalytic test approximatively by 1 nm, by comparison with the reduced sample. This more important sintering effect observed on the samples at high Ni loading is obviously related to initial NPs surface density which is higher for high loading samples. It results in a higher probability of NPs encounter and growth during reaction. Interestingly, the Ni average particles size remains far below the average pores size of the catalysts, showing that the confinement effect occurring when a limited interaction between Ni phase and silica surface exists,[55] does not occur for the Ni_X% catalysts, indicating a stronger interaction between the generated Ni based particles and the silica surface.

(iii) The micrographs do not allow to easily detect the formation of a carbon phase, except in the case of Ni_40% for which few carbon nanofilaments are found between the silica grains (TEM image at low magnification, Figure 9). In previous work, -OH surface groups of remaining unreduced PS phase were identified to possibly serve as sites for Ni NPs stabilization at low size, that can result in decrease in carbon formation, thereby enhancing the

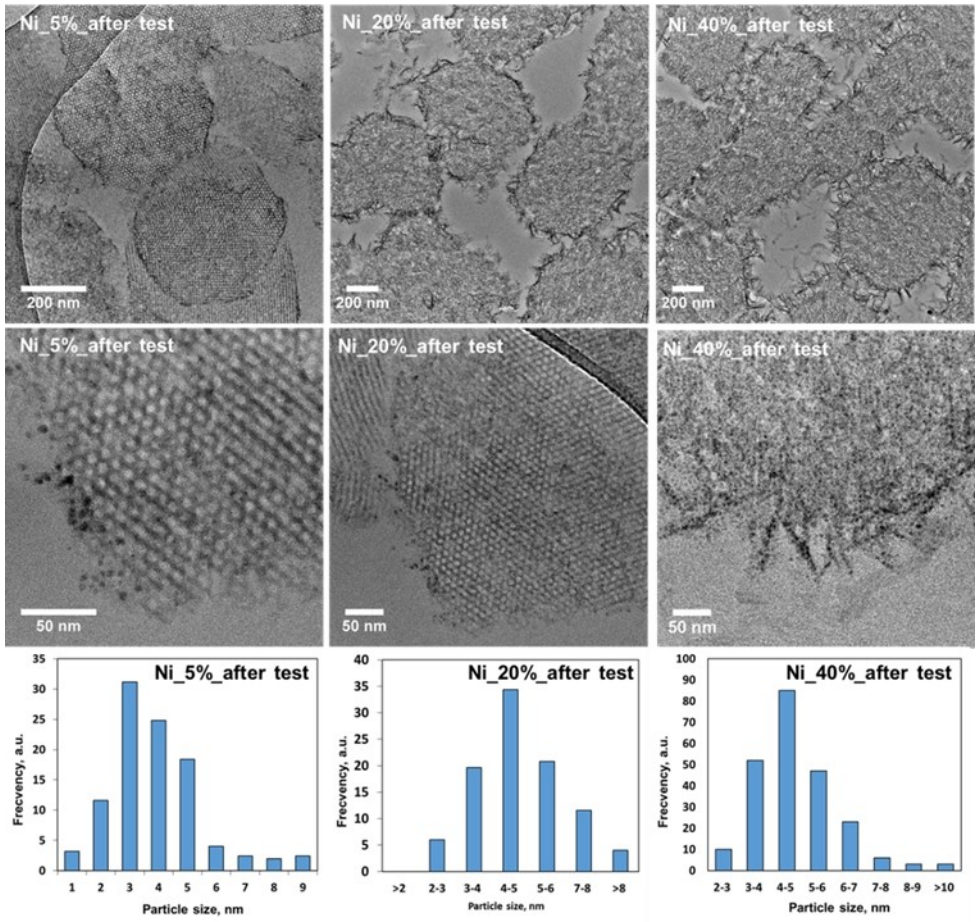


**Figure 9.** TEM images collected on Ni_5%, Ni_20%, and Ni_40% samples after catalytic test without pretreatment before reaction. Conditions: $CH_4/CO_2 = 1$, 20% $CH_4$, reaction performed 5 h at 600 °C followed by 5 h at 700 °C.

catalytic stability.[46] Our results confirm that low size Ni NPs are active and are not prone to produce carbon phase.

XPS analyses performed on the Ni_20% sample after DRM at 700 °C in $CH_4/CO_2 = 1$ and 20% of $CH_4$ without *in situ* pretreatment in $H_2$ of the catalyst (Ni-20%_after test) are shown in Figure 5, Figure S14 and Table S3. When compared with the reduced catalyst (Figure 5c), the Ni $2p_{3/2}$ core level evidences the presence of a large majority of $Ni^{2+}$ cations (Figure 5). As a consequence, a $Ni^0/Ni^{2+}$ surface ratio $\leq 0.1$ is obtained by XPS analysis, much lower compared to the one obtained after reduction at 700 °C. The O 1s core level displays a main contribution at 533.2 eV (Figure 5) fitting with the presence of $O^{2-}$ species from silica framework.[50] No notable modifications of either the Si 2p (103.7 eV; $Ni2p_{3/2}$-Si2p B.E. of 752.9 eV) or C 1 s (284.8 eV) core levels can be observed between the states after and before reaction. In particular, the XPS analysis of C 1 s region does not reveal any extra formation of carbon species during the reaction.

By increasing the metal loading the agglomeration of the NPs, mostly at the external part of the silica grain is observed, is the case of Ni_20%. As already discussed in Section 3.2.1 Catalysts in the oxidized state, the high metal loading of 40% is inducing also the generation of another pore size of 4.1 nm, the mesoporosity of the silica is completely disappeared. Nevertheless, even if the metal loading is high the NPs size is maintained between 3 and 4 nm, the density of the NPs is extremely high, from here the better catalytic performances for this sample. As consequence, the appearance of some carbon filaments is observed after 5 h of reaction. The proof of the size to density of NPs at the surface of the catalyst is strength by the stability test which is definitely showing high resistance toward the production of carbon.

Considering whole characterization results, it seems reasonable to assume that the promoting effect on the catalytic activity when the reduction temperature increases for Ni_20%, while a slight negative effect is observed for Ni_40%, originate from the thermal stability of the different catalysts, as already observed.[45] However, always on the basis of the results, a very limited variation of dispersion occurs meaning that the accessibility of the Ni particles is maintained for the reaction, and explaining why limited deactivation occurs even at high Ni loading in the catalysts.[56] Additionally, results demonstrate a limited accumulation of carbon on the catalysts, showing that the preparation of low size Ni NPs is an efficient strategy to maintain catalyst stability avoiding side reactions. Considering the results from the literatures (listed in Table S4) obtained in comparable Ni metal

loading, the results presented in this study are showing great resistance toward sintering for high metal loading. The conversions for $CO_2$ and $CH_4$ are showed to be 10 to 20% higher in similar reaction conditions for dry reforming of methane. As the performance in DRM is counted in the resistance toward the carbon formation, while, the spent catalysts are showing limited carbon production, while excellent results are showed for the Ni_20% over stability test, by comparison with the literature.[43]

## Conclusions

Ni catalysts, issued from reduction of phyllosilicate phase obtained by deposition-precipitation of nickel over SBA-15 type silica, are prepared at four different Ni loadings (5, 10, 20 and 40 wt.%). Characterization evidenced the complete incorporation of the nickel inside the phyllosilicate phase. Compared to classical impregnation route is resulting in high amount of Ni, deposed onto the silica, superior to 20 wt.%. However, significant modifications of the SBA-15 pore topology occur during synthesis step, with, for material highly loaded in nickel (40 wt.%), an almost complete destruction of the initial ordered pore structure. Nevertheless, quite high surface areas, $>300\ m^2 g^{-1}$, and open porosities are retained. Temperature programmed reduction, as well as *in situ* XRD experiments performed under $H_2$, evidenced a high stability toward reduction of the materials even if lower than obtained for classical 2:1 phyllosilicate synthesized by hydrothermal procedure. TEM analysis showed the formation of relatively fine and homogeneous population of Ni particles, even for the highly loaded catalysts. Then, for the 40 wt.% Ni sample, the reduction at 800 °C results in the formation highly dispersed metallic particles of ~4 nm. These Ni particles are unequally distributed on the silica surface at low loading. At Ni loading $\leq$10 wt.%, an enrichment of Ni particles on the periphery of the silica grains is observed, due to the growth of the phyllosilicate filaments at the external surface of the silica forming urchin-like morphology. Ni NPs distribution equilibrate when nickel loading increases to 20–40 wt.%. Consequently, the DP method is allowing to produce highly dispersed metallic phases of nickel, even at 40 wt.%, where the presence of 1:1 type phyllosilicate is observed, in the benefit of lower reduction temperature, thus economically effective from energy consuming point of view.

Excellent properties in the dry reforming of methane reaction are obtained for all Ni_X% sample, performances obtained outperforming the $LaNiO_3$ reference catalyst. *In situ* pretreatment under $H_2$ (600 °C–700 °C) is not a necessity to perform the reaction, and the catalyst can be activated under reaction to obtain conversions comparable to those of the *in situ* pre-treated catalyst. The best performances are obtained for the Ni_40% catalyst: at 600 °C, $X_{CH4}=27\%$ and $X_{CO2}=37\%$; at 700 °C, $X_{CH4}=57\%$ and $X_{CO2}=68\%$. Very limited carbon accumulation and limited Ni particles sintering occur in reaction that explains why stability in reaction is observed. Additionally, Ni_20% was tested in reaction, using undiluted flow (50% $CH_4$, 50% $CO_2$). The catalyst demonstrates good activity and stability under these more severe conditions confirming the excellent capabilities of the Ni-$SiO_2$ catalysts when prepared from Ni-phyllosilicate phase exsolution. The stability test for 80 h under DRM is proving the high resistance toward sintering and carbon formation for Ni_20%.

## Experimental Section

### Catalyst preparation

Chemicals for the syntheses in this work (SBA-15 silica support, transition metal containing catalysts) were used without any modifications: tetraethylorthosilicate ($Si(OC_2H_5)_4$, TEOS, 98 wt.%, Sigma-Aldrich), Pluronic P123 (a non ionic triblock copolymer poly(ethylene oxide)-block-poly(propylene oxide)-blockpoly(ethylene oxide)-block, $PEO_{20}PPO_{70}PEO_{20}$, M = 5800 g, BASF Corp.), hydrochloric acid (HCl, 37 wt.%, Sigma-Aldrich), nickel nitrate hexahydrate ($Ni(NO_3)_2 6H_2O$, 98 wt.%, Sigma-Aldrich), urea ($CO(NH_2)_2$ >99.0 wt.%, Sigma-Aldrich, ACS reagent), lanthanum nitrate hexahydrate ($La(NO_3)_3 6H_2O$, 99.5 wt.%, Sigma), citric acid ($C_6H_8O_7$, 99 wt.%, Acros), nickel chloride ($NiCl_2 6H_2O$, 98 wt.%, Sigma Aldrich), sodium metasilicate ($Na_2SiO_3$, 98 wt.%, Sigma Aldrich).

The SBA-15 porous support is prepared according to a classical procedure.[57] For the synthesis, a solution consisting of HCl solution (150 mL, 1.6 M) and the polymer of P123 (4.00 g) is prepared. After well mixing at 40 °C for 6 h, the silica source is added dropwise (TEOS, 8.5 g) and the solution is maintained for ageing for 24 h. A hydrothermal treatment at 100 °C is then performed into a teflon-lined autoclave for 48 h. The solid support was recovered by filtration and washed with deionised water in order to eliminate any traces of Cl. Thermal steps included a drying step at 80 °C (12 h) for solvent evaporation and the calcination step (for the P123 porogen elimination) performed under static air at 550 °C during 6 h (temperature increase rate = 1.5 °C $min^{-1}$), finally the support with empty pores is obtained and denoted SBA-15.

The phyllosilicate derived phases were obtained via Deposition Precipitation (DP) approach.[30] The synthesis is taking place in a thermostated reactor, as silica source is used the calcined SBA-15 support (1.00 g), an aqueous solution of nickel nitrate hexahydrate (0.14 mol $L^{-1}$) is added to the mixture. In order to obtained high loading of Ni over the $SiO_2$, the metallic phase is comprised between 5 wt.% and 40 wt.%. In order to increase the pH from the same initial point we use nitric acid was employed up to the value of 2.0. Then, the temperature of the solution was stabilized at 90 °C and the urea solution (3 mol $L^{-1}$) was added dropwise. The solution was stirred at 90 °C during 24 h, in these conditions, the release of ammonia into the solution is taking place slowly, permitting to form the phyllosilicate phases well dispersed onto the SBA-15 surface. At the end of the ageing step, a pH of $7.4\pm0.1$ was observed. The Ni-containing solids, recovered by filtration, were washed with deionised water, to eliminate the impurities, before being dried 12 h at 40 °C. Activation step consists in a thermal treatment at 500 °C (6 h, temperature increase rate of 1.5 °C $min^{-1}$) under air in a muffle oven. Calcined Ni-containing solids are denoted Ni_X%, where X refers to the theoretical Ni loading (X = 5, 10, 20, 40 wt.%). the ICP analysis is giving relatively close values (X = 5, 12, 22, 42 wt.%) to the calculated ones. Prior to the DRM catalytic test, the calcined samples were reduced in pure $H_2$ atmosphere at temperatures of 600 to 800 °C and characterized. These temperatures were selected after analyzing the TPR profiles.

Two references materials were added to the study: 2:1 Ni-phyllosilicate synthesized according to conventional hydrothermal procedure, and denoted PS 2:1,[36] to confirm the interest of starting from porous silica to obtained active metallic NPs of smaller size and

for the prove whether the formation of this phase is occurring when DP condition;

- $LaNiO_3$ perovskite material was also prepared by the classical citrate complexation method,[32] for DRM comparison.[32]

### Dry reforming of methane reaction

The catalytic reaction was conducted in a fixed-bed "up flow" tubular quartz reactor (inner diameter: 4 mm for 10 mg and 8 mm for 50 mg of catalyst deposit on the frit). Reaction was conducted at atmospheric pressure. Catalytic bed temperature was controlled using a programmer, with a thermocouple positioned in close contact with the catalytic bed. When mentioned, the catalyst was previously *in situ* treated under pure $H_2$ flow at T = 600–700 °C for 10 h, it will be used the notation DRM-t, where t = 600 or 700. It was previously shown that 10 h pretreatment is not affecting the NPs size. The reactions were performed under diluted conditions and $N_2$ was selected as carrier gas. The reaction was carried out with a $CH_4$/$CO_2$ molar ratio of 1, and varying $CH_4$ and $CO_2$ concentrations (20% – dilute conditions, to 50% - non diluted reaction). The total flow rate was fixed at 80 mL min$^{-1}$. The parameters chosen for DRM reaction were previously tested in order to remove any external and internal diffusions. Concentrations of reactants and products were measured by using a gas chromatograph from Thermo Scientific (TRACE GC ULTRA model) equipped with a flame ionization detector (FID) and a thermal-conductivity detector (TCD).Catalytic performances reported here were obtained under steady state conditions, after 5 h of stabilization at the selected temperature. $CH_4$ conversion ($X_{CH4}$), $CO_2$ conversion ($X_{CO2}$), products molar compositions ($C_i$, dry basis) and $H_2$/CO molar ratio were obtained using formula presented in Equations (7–10).

$$X_{CH_4} = \frac{(CH_{4\,in} - CH_{4\,out})}{CH_{4\,in}} \times 100\,\% \quad (7)$$

$$X_{CO_2} = \frac{(CO_{2\,in} - CO_{2\,out})}{CO_{2\,in}} \times 100\,\% \quad (8)$$

$$C_i = \frac{n_i}{\sum_{products} n_i} \text{ x } 100\,\% \quad (9)$$

$$H_2/CO \text{ ratio} = F^{out}_{H_2}/F^{out}_{CO} \quad (10)$$

Where $F^{out}_{H_2}$ and $F^{out}_{CO}$ correspond to the flow rates of each component in the effluent.

$N_2$-physisorption at −77 K was used to evaluate the textural properties, for this the materials were analyzed by on a Micromeritics Tristar II automated gas sorption system. For the measure were used 50 mg of TGA sample which were prior treated under dynamic vacuum at 300 °C for 3 h, in order to eliminate any traces of water or impurities. The textural parameters were calculated by using Tristar Plus II 4.06 software. Specific surface area was calculated using the B.E.T. algorithm, in the $P/P_0$ range from 0.10 to 0.25, t-plot method was used to evaluate the micropore volume and surface area (de Boer statistical thickness $t$ = 3.8–6.5 Å), the mesopore size distribution was obtained using the NLDFT equilibrium algorithm for cylindrical pores and the pore volume is determined at $P/P_0$ = 0.95, on the adsorption branch.

Wide angle XRD patterns were carried out on a Panalytical Empyrean X-ray system, in Bragg Benttano configuration (Cu Kα radiation, λ = 1.54184 Å). Acquisition program was: $10° < 2\theta < 80°$, step size = 0.05°, step time = 120 s. ICDD database was used for crystalline phase identification. The Scherrer equation, $D = K\lambda/b.\cos\theta$, was used for crystal domain size determination (where: K is a structure constant (value of 0.9 for spherical crystals), λ is the incident X-ray wavelength, b is the FWHM of the peak after correction for instrumental broadening and θ is the Bragg angle.

*In-situ* XRD under $H_2$ was performed on a Bruker D8 ADVANCE X-ray system (Cu Kα radiation, λ = 1.54184 Å), the purpose is to reveal the evolution of the phases, in the same reduction conditions as used for TPR analysis. The diffractometer was equipped with a VANTEC-1 detector. Kanthal (FeCrAl) filament cavity were used for analysis. The Kanthal is giving two intense peaks at 2 theta of 43.57° and 63.87°, which are not taking into consideration for the further interpretation of the diffractograms. Program applied for the reduction consisted in: 30 mL min$^{-1}$ of 3.0 vol.% $H_2$ in He in the range of temperature from 30 °C to 800 °C (rate = 10 °C min$^{-1}$). Conditions selected for diffractogram registration were: $10° < 2\theta < 80°$ with a step size = 0.05° and step time = 2 s. "In the graph, the diffractograms are offset with by the distance indicated on each graph."

TEM Micrographs were collected on a JEOL 2100 UHR instrument (200 kV, with a $LaB_6$ source and equipped with a Gatan Ultra scan camera). The microscope was equipped with an Energy Dispersive X-ray Spectroscopy (EDXS) detector. Samples were included in spurr resin and by ultramicrotomy were cut in samples of 50 nm width. The samples were thereby positioned onto carbon grids for analysis. The images were collected for the samples in oxidized form, in reduced form at 600 °C and at 800 °C, and finally for the spent samples collected after catalytic test (for observing the eventual carbonaceous formation). For the presentation of the TEM images and for measuring the nanoparticle size, ImageJ software was used. The histograms were made by a total number of 250 particles measured on different TEM images.

$H_2$-TPR experiments were obtained on Autochem-type system from Micromeritics. Gas phase $H_2$ concentration was on-line monitored on a TCD. $H_2$-TPR runs were conducted under a 3 vol.% $H_2$ in Ar flow. For the analysis 50 mg of sample was placed in and "U" shape reactor. Prior to the reduction step the samples were pretreated at 500 °C in air flow in order to remove any impurities. For the reduction, the following conditions were adopted: the $H_2$ flow rate of 50 mL min$^{-1}$, the profiles were registered at temperatures from 25 °C to 900 °C (rate = 10 °C min$^{-1}$).

TGA measurements were carried out on a SDT Q600 TA Instrument. The experiments were performed under air at a total flow rate of 100 mL min$^{-1}$ for temperatures from 25 °C to 1000 °C (10 °C min$^{-1}$). The quantity used for the analysis is of 10 mg. The weight loss was calculated using Thermal Analysis software.

XPS analyses were conducted on a Kratos Analytical AXIS Ultra$^{DLD}$ spectrometer. The system was equipped with a monochromatic Al X-ray source (1486.6 eV) working at a pass energy of 40 eV. The powder samples was deposited on a copper holder. Position of C 1s adventitious carbon contribution was fixed at binding energy (BE) = 284.8 eV. Data treatments were conducted on the CasaXPS software.

## Acknowledgements

*Y. Wei gratefully acknowledges China Scholarship Council CSC for PhD granting. The authors would like to thank L. Burylo (XRD), M. Trentesaux and P. Simon (XPS), and S. Pronier (TEM), Véronique Alaimo (ICP). Chevreul Institute (FR 2638), Ministère de l'Enseignement Supérieur, de la Recherche et de l'Innovation, Hauts-de-*

*France Region and FEDER are acknowledged for supporting and funding partially this work.*

## *Conflict of Interests*

The authors declare no conflict of interest.

## Data Availability Statement

The data that support the findings of this study are available from the corresponding author upon reasonable request.

**Keywords:** $CH_4$, dry reforming · hydrogen, nanoparticles · phyllosilicate, transition metal

[1] Z. Li, Q. Lin, M. Li, J. Cao, F. Liu, H. Pan, Z. Wang, S. Kawi, *Renew. Sustain. Energy Rev.* **2020**, *134* 110312.
[2] J. Rogelj, M. den Elzen, N. Höhne, T. Fransen, H. Fekete, H. Winkler, R. Schaeffer, F. Sha, K. Riahi, M. Meinshausen, *Nature* **2016**, *534*, 631.
[3] W. J. Jang, J. O. Shim, H. M. Kim, S. Y. Yoo, H. S. Roh, *Catal. Today* **2019**, *324*, 15.
[4] A. Abdulrasheed, A. A. Jalil, Y. Gambo, M. Ibrahim, H. U. Hambali, M. Y. S. Hamid, *Renew. Sustain. Energy Rev.* **2019**, *108*, 175.
[5] Y. Gao, J. Jiang, Y. Meng, F. Yan, A. Aihemaiti, *Energy Convers. Manag.* **2018**, *171*, 133.
[6] G. Zhang, J. Liu, Y. Xu, Y. Sun, *Int. J. Hydrogen Energy* **2018**, *43*, 15030.
[7] Z. Li, S. Das, P. Hongmanorom, N. Dewangan, M .H. Wai, S. Kawi, *Catal. Sci. Technol.* **2018**, *8*, 2763.
[8] Z. Li, Z. Wang, S. Kawi, *ChemCatChem* **2019**, *11*, 202.
[9] M. Usman, W. M. A. Wan Daud, H. F Abbas, *Renew. Sustain. Energy Rev.* **2015**, *45*, 710.
[10] X. Yan, T. Hu, P. Liu, S. Li, B. Zhao, Q. Zhang, W. Jiao, S. Chen, P. Wang, J. Lu, L. Fan, X. Deng, Y. X. Pan, *Appl. Catal. B* **2019**, *246*, 221.
[11] S. Das, J. Ashok, Z. Bian, N. Dewangan, M. H. Wai, Y. Du, A. Borgna, K. Hidajat, S. Kawi, *Appl. Catal. B* **2018**, *230*, 220.
[12] F. Wang, B. Han, L. Zhang, L. Xu, H. Yu, W. Shi, *Appl. Catal. B* **2018**, *235*, 26.
[13] A. R. Bawah, Z. O. Malaibari, O. Muraza, *Int. J. Hydrogen Energy* **2018**, *43*, 13177.
[14] A. A. S. Oliveira, R. L. B. A. Medeiros, G. P. Figueredo, H. P. Macedo, R. M. Braga, F. V. Maziviero, M. A. F. Melo, D. M. A. Melo, M. M. Vieira, *Int. J. Hydrogen Energy* **2018**, *43*, 9696.
[15] M. Lia, A. C. van Veen, *Appl. Catal. B* **2018**, *237*, 641–648.
[16] P. G. Lustemberg, P. J. Ramírez, Z. Liu, R. A. Gutiérrez, D. G. Grinter, J. Carrasco, S. D. Senanayake, J. A. Rodriguez, M. V. Ganduglia-Pirovano, *ACS Catal.* **2016**, *6*, 8184–8191.
[17] Z. Liu, P. Lustemberg, R. A. Gutiérrez, J. J. Carey, R. M. Palomino, M. Vorokhta, D. C. Grinter, P. J. Ramírez, V Matolín, M. Nolan, Ganduglia M. V. Pirovano, S. D. Senanayake, J. A. Rodriguez, *Angew. Chem. Int. Ed.* **2017**, *56*, 13041.
[18] L. Jalowiecki-Duhamel, H. Zarrou, A. D'Huysser, *Int. J. Hydrogen Energy* **2008**, *33*, 5527.
[19] L. Jalowiecki-Duhamel, H. Zarrou, A. D'Huysser, *Catal. Today* **2008**, *138*, 124.
[20] D. Guo, Y. Lu, Y. Ruan, Y. Zhao, Y. Zhao, S. Wang, X. Ma, *Appl. Catal. B* **2020**, *277*, 119278.
[21] A. L. A. Marinho, A. C. Rabelo-Neto, F. Epron, N. Bion, F. S. Toniolo, F. B. Noronha, *Appl. Catal. B* **2020**, *268*, 118387.
[22] K. Li, C. Pei, X. Li, S. Chen, X. Zhang, R. Liu, J. Gong, *Appl. Catal. B* **2020**, *264*, 118448.
[23] Y. Wang, L. Yao, S. Wang, D. Mao, C. Hu, *Fuel Process. Technol.* **2018**, *169*, 199.
[24] K. Sutthiumporn, S. Kawi, *Int. J. Hydrogen Energy* **2011**, *36*, 14435.
[25] Sietsma, J. D. Meeldijk, J. P. den Breejen, M. Versluijs-Helder, A J. R. A. J. van Dillen, P. E. de Jongh, K. P. de Jong, *Angew. Chem. Int. Ed.* **2007**, *46*, 4547.
[26] H. Friedrich, J. R. A. Sietsma, P. E. de Jongh, A. J. Verkleij, K. P. de Jong, *J. Am. Chem. Soc.* **2007**, *129*, 10249.
[27] J. W. Geus, *Stud. Surf. Sci. Catal.* **1983**, *16*, 1–33.
[28] N. Wang, W. Chu, T. Zhang, X. S. Zhao, *Int. J. Hydrogen Energy* **2012**, *37* (1), 19.
[29] T. Lehman, T. Wolff, C. Hamel, P. Veit, B. Garke, A. Seidel-Morgenstern, *Microp. Mesop. Mater.* **2012**, *151*, 113.
[30] C. Ciotonea, B. Dragoi, A. Ungureanu, A. Chirieac, S. Petit, S. Royer, E. Dumitriu, *Chem. Commun.* **2013**, *49*, 7665.
[31] P. Burattin, M. Che, C. Louis, *J. Phys. Chem. B* **1998**, *102*, 2722.
[32] J. P. Dacquin, D. Sellam, C. Batiot-Dupeyrat, A. Tougerti, D. Duprez, S. Royer, *ChemSusChem* **2014**, *7*, 631.
[33] S. Kawi, Z. Bian, *Catal. Today* **2020**; *339*, 3.
[34] S. Royer, D. Duprez, F. Can, X. Courtois, C. Batiot-Dupeyrat, S. Laassiri, H. Alamdari, *Chem. Rev.* **2014**, *114*, 10292.
[35] R. C. Rabelo-Neto, H. B. E. Sales, C. V. M. Inocéncio, E. Varga, A. Oszko, A. Erdohelyi, F. B. Noronha, L. V. Mattos, *Appl. Catal. B* **2018**, *221*, 349.
[36] A. Albarazi, P. Beaunier, P. Da Costa, *Int. J. Hydrogen Energy* **2013**, *38*, 127.
[37] J. Juan-Juan, M. C. Román-Martínez, M. J. Illán-Gómez, *Appl. Catal. A* **2009**, *355*, 27.
[38] K. Jabbour, P. Massiani, A. Davidson, S. Casale, N. El Hassan, *Appl. Catal. B* **2017**, *201*, 527.
[39] L. Qian, Z. Ma, Y. Ren, H. Shi, B. Yue, S. Feng, J. Shen, *Fuel* **2014**, *122*, 47.
[40] O. Omoregbe, H. T. Danh, C. Nguyen-huy, H. D. Setiabudi, S. Z. Abidin, Q. Duc, D. V. N. Vo, *Int. J. Hydrogen Energy* **2017**, *42*, 11283.
[41] V. Arcotumapathy, D. V. N. Vo, D. Chesterfield, C. T. Tin, A. Siahvashi, F. P. Lucien, A. A. Adesina, *Appl. Catal. A* **2014**, *479*, 87.
[42] C. Batiot-Dupeyrat, F. Martinez-Ortega, M. Ganne, J. M. Tatibouët, *Appl. Catal. A* **2001**, *206*, 205.
[43] M. Kosari, S. Askari, A. M. Seayad, S. Xi, S. Kawi, A. Borgna, H. C. Zeng, *Appl. Catal. B* **2022**, *310*, 121360.
[44] N. Wang, X. Yu, Y. Wang, W. Chu, M. Liu, *Catal. Today* **2013**, *212*, 98.
[45] J. C. Park, H. J. Lee, J. U. Bang, K. H. Park, H. Song, *Chem. Commun.* **2009**, *47*, 7345.
[46] M. V. Sivaiah, S. Petit, M. F. Beaufort, D. Eyidi, J. Barrault, C. Batiot-Dupeyrat, S. Valange, *Microp. Mesop. Mater.* **2011**, *140*, 69.
[47] B. Dragoi, A. Ungureanu, C. Ciotonea, A. Chirieac, S. Petit, S. Royer, E. Dumitriu, *Micropor. Mesopor. Mater.* **2016**, *224*, 176.
[48] A. Ungureanu, B. Dragoi, A. Chirieac, C. Ciotonea, S. Royer, D. Duprez, A. S. Mamede, E. Dumitriu, *ACS Appl. Mater. Interf.* **2013**, *5*, 3010.
[49] M. C. Biesinger, B. P. Payne, A. P. Grosvenor, L. W. M. Lau, A. R. Gerson, R. St. C. Smart, *Appl. Surf. Science* **2011**, *257*, 2717.
[50] Y. Qi, Z. Yang, T. Chen, Y. Xi, J. Zhang, *Appl. Surf. Sci.* **2020**, *501*,144165.
[51] A. R. Bawah, Z. O. Malaibari, O. Muraza, *Int. J. Hydrogen Energy* **2018**, *43*, 13177.
[52] Q. Zhang, M. Wang, T. Zhang, Wang, X. Tang, P. Ning, *RSC Adv.* **2015**, *5*, 94016.
[53] J. W. E. Coenen, *Appl. Catal.* **1991**, *75*, 193.
[54] C. Ciotonea, B. Dragoi, A. Ungureanu, E. Marceau, H. Alamdari, S. Petit, E. Dumitriu, S. Royer, *Catal. Sci. Technol.* **2017**, *7*, 5448.
[55] W. Yang, H. Liu, Y Li, H. Wu, D. He, *Int. J. Hydrogen Energy* **2016**, *41*,1513.
[56] S. Kweon, Y. W. Kim, D. Jo, C–H. Shin, M. B. Park, H. K. Min, *Micropor. Mesopor. Mater.* **2022**, *332*, 111683.
[57] H. Lin, X. Zhong, C. Ciotonea, X. Fan, X. Mao, Y. Li, B. Deng, H. Zhang, S. Royer, *Appl. Catal. B* **2018**, *230*, 1.

Manuscript received: February 9, 2023
Revised manuscript received: June 1, 2023
Accepted manuscript online: June 6, 2023
Version of record online: June 28, 2023